Weierstraß-Institut

für Angewandte Analysis und Stochastik

Leibniz-Institut im Forschungsverbund Berlin e. V.

Modeling high resolution MRI: Statistical issues with low SNR

Jörg Polzehl[1], Karsten Tabelow[1]

submitted: November 17, 2015

[1] Weierstrass Institute
    Mohrenstr. 39
    10117 Berlin
    Germany
    E-Mail: joerg.polzehl@wias-berlin.de
            karsten.tabelow@wias-berlin.de

Noise is a common issue for all Magnetic Resonance Imaging (MRI) techniques and obviously leads to variability of the estimates in any model describing the data. A number of special MR sequences as well as increasing spatial resolution in MR experiments further diminish the signal-to-noise ratio (SNR). However, with low SNR the expected signal deviates from its theoretical value. Common modeling approaches therefore lead to a bias in estimated model parameters. Adjustments require an analysis of the data generating process and a characterization of the resulting distribution of the imaging data. We provide an adequate quasi-likelihood approach that employs these characteristics. We elaborate on the effects of typical data preprocessing and analyze the bias effects related to low SNR for the example of the diffusion tensor model in diffusion MRI. We then demonstrate that the problem is relevant even for data from the Human Connectome Project, one of the highest quality diffusion MRI data available so far.

1 Introduction

Many recent advances in Neuroscience are closely related to imaging techniques that allow for an in-vivo examination of the human brain. Magnetic Resonance Imaging (MRI) has played and is playing an essential role in this process due to its inherent non-invasiveness. This property is in contrast to other imaging techniques like Positron Emission Tomography (PET) or Computer Tomography (CT) that require potential harmful high energy radiation during imaging. Furthermore, MRI, unlike, e.g., electroencephalography (EEG) or magnetoencephalography (MEG), provides a reasonable temporal **and** spatial resolution. And last but not least, its versatile image contrasts enable many different looks into the brain focusing on different tissues and their properties. For an excellent introduction into the physics of MRI see, e.g., Callaghan [1991].

MRI like any imaging technique suffers from specific artifacts, that affect data analysis in neuroscientific research or clinical applications. Among those the most important are magnetic susceptibility artifacts, registration problems or eddy-current distortions for sequences with large, rapidly switched magnetic field gradients [Johansen-Berg and Behrens, 2009]. Artifact correction of MRI data can be performed by various methods, see, e.g., Mohammadi et al. [2010] or Ruthotto et al. [2012] and the references therein for recent developments. In this paper we are focusing on the influence of image noise as one of the limiting factors for increasing the spatial resolution in MRI [Edelstein et al., 1986]. Despite introducing variability into the estimates in any model describing the data low signal-to-noise ratio (SNR) leads to the deviation of the expected signal from its theoretical value which induces also a bias.

One of the MR image contrasts that is especially prone to low SNR is diffusion weighted imaging [dMRI; Jones, 2010] which examines the diffusional properties of the omnipresent water

in the brain. The experimental setup allows for probing different diffusion directions and thus accessing the anisotropy which has shown to be directly related to the underlying tissue geometry, see, e.g., Johansen-Berg and Behrens [2009]. From dMRI data a lot of interesting measures based on a number of different diffusion models describing the directional dependence of the data have been derived [Assemlal et al., 2011]. Examples include scalar maps of the local diffusion anisotropy or vector fields of main diffusion directions pointing along elongated tissue structures in the brain [Johansen-Berg and Behrens, 2009, Jones, 2010]. These measures have been shown to be relevant not only for research on the normal brain but also for clinical decision making on neurological diseases, like epilepsy or Multiple Sclerosis [Deppe et al., 2007, Kleffner et al., 2008, Deppe et al., 2013].

Another recent acquisition protocol potentially susceptible to low SNR is quantitative multi-parameter mapping [MPM; Weiskopf et al., 2013, 2014], which is designed to provide standardized information about tissue microstructure. It relates measurements with different MR contrasts and at multiple echo times within a model derived from MR physics. The model parameters are supposed to be comparable across time points and imaging sites enabling the search for diagnostic markers for neuronal diseases in group studies, see, e.g., [Weiskopf et al., 2013] and references therein. As for dMRI increasing image resolution inherently lowers the SNR. If not accounted for, the resulting bias compromises the comparability of estimated model parameters.

Without loss of generality we will in this paper focus on diffusion MRI and use corresponding models and acquired data in our discussion. However, the conclusions apply to any other MR acquisition with low SNR and any other common modelling approach for the data.

It is long known, that noise in dMRI leads to a bias in the estimates of diffusion model parameters [Gudbjartsson and Patz, 1995, Pierpaoli and Basser, 1996, Basser and Pajevic, 2000, Jones and Basser, 2004]. The effect gets more severe with diminishing signal-to-noise ratio (SNR), e.g., as a consequence of increased spatial resolution and/or higher diffusion-weighting of the dMRI data. In this paper, we want to shed further light into the "bias problem" in dMRI data analysis and its possible solutions from a statistical perspective. We provide a statistical approach to characterize and correctly treat the noise when modeling MRI data. We will analyze the influence of data processing, e.g., for artifact correction, on such solutions and argue, how the noise properties of the original unprocessed data are relevant to the treatment of the bias problem. This is important as data processing generally increases the SNR by means of local averages such that the problem is often not recognized in practice. We will demonstrate the issues using one of the highest quality dMRI data available so far, namely the data from the Human Connectome Project (HCP), see `http://www.humanconnectomeproject.org/`. In this sense, it is a generic problem for all dMRI data.

2 Statistical properties of MRI data

In the process of data acquisition for MRI a receiver coil basically receives radio-frequency signals related to precessing nuclear spins; the frequency domain of these signals is usually denoted as k-space. The generation of images in the spatial domain is then performed by inverse

Fourier-transform of the complex-valued k-space data, followed by the formation of a magnitude image, see Callaghan [1991] for an introduction. The manner in which k-space is sampled is subject of intense research, in this paper we consider for simplicity Cartesian acquisitions in k-space, only.

k-space data from a single receiver coil is commonly considered to be complex Gaussian distributed; the signal in the magnitude image then has a Rician distribution [Rice, 1944, Gudbjartsson and Patz, 1995], which is a re-scaled non-central χ-distribution with 2 degrees of freedom. The skewness of this distribution leads to a difference between the expectation value of the signal and the true noise-less signal [Henkelman, 1985]; consequently the mean signal in the background of an MR image with no spins at all does not vanish.

To increase the sensitivity of the data acquisition parallel imaging methods have been introduced [Roemer et al., 1990]. There, data from multiple receiver coils are combined for increased SNR and homogeneous coverage. To speed up acquisition several modifications are used in parallel imaging protocols, e.g. subsampling in K-space, reduced field of view, multi slice acquisitions, partial parallel acquisitions, e.t.c.. All these methods introduce different types of spatial correlation in the acquired image data, see e.g. Bruce et al. [2011], Bruce et al. [2012], or Bruce and Rowe [2014], and together with the image reconstruction methods determine the statistical distribution of the image data.

The reconstruction of the image from multiple coil data can be done using various methods. As an example a sum-of-squares (SoS) combination of the k-space data from multiple receiver channels [Roemer et al., 1990] simply calculates a quadratic mean of the amplitudes derived from each channel. The distribution of the image signal S then becomes a non-central χ-distribution with $2L$ degrees of freedom:

$$S/\sigma \sim \chi_{2L}(\zeta/\sigma),$$

where L is the number of receiver coils, ζ is the true noise-less signal and σ is the standard deviation of the complex Gaussian distribution of the k-space data. While this provides a simple statistical description the reconstruction does not efficiently use the available information on the data from the receiver coils.

In general, data from the different receiver coils is correlated [Hayes and Roemer, 1990]. Signal intensity varies with the distance to the respective receiver coil. As a consequence the image signal distribution obtained by image reconstruction methods that account for these properties is still approximately non-central χ, however, with a smaller effective number $2L_{eff}$ degrees of freedom [Aja-Fernández and Tristán-Vega, 2012]. A similar result has been obtained [Aja-Fernández et al., 2011] for MRI data using Generalized Autocalibrating Partially Parallel Acquisition [GRAPPA; Griswold et al., 2002] that reconstructs images from sub-sampled k-space data in each coil.

Alternatively, a SENSE (Sensitivity Encoding for Fast MRI) [Pruessmann et al., 1999] reconstruction is a weighted mean of the single coil data using location dependent sensitivity maps as weights with an undersampling factor R. A special refinement for $R = 1$ is known as SENSE1 [Sotiropoulos et al., 2013b] and used as standard protocol in the Human Connectome Project [Sotiropoulos et al., 2013a]. As the combination of the multiple coil data is performed linearly in k-space already, the signal distribution of the image data can be expected to be of

Rician form.

In this paper we will henceforth consider a non-central χ-distribution for the signal with $2L_{eff}$ degrees of freedom using an effective, and location-dependent, number of coils. When considering HCP data in our example section, we will be able to specify $L_{eff} = 1$. The magnitude signal distribution is restricted to the positive axis and hence possesses skewness, i.e., $\zeta < \mathrm{E}S$. The difference between the parameter ζ and the expectation of the signal increases with decreasing SNR of the data.

In a typical dMRI sequence multiple volumes of data are acquired for a suitable sample of diffusion gradient directions to probe the directional dependence of the diffusion signal [Jones, 2010]. This automatically generates an image registration problem, as the subject is in general constantly moving in the scanner during data acquisition, at least due to physiological pulsation. In a similar manner discontinuities of bulk magnetic susceptibility and eddy currents caused by the rapid switching of magnetic field gradients produce spatial distortions in the images. If not corrected for, strong artifacts of this kind diminish the quality of the data and hinder data analysis. The correction methods for spatial distortions in the data, however, automatically involve signal interpolations, that along the way reduce the signal variability. These interpolations generally preserve the relation between expected and the theoretical (noise-free) signal, which is determined by the SNR of the unprocessed data.

3 Modeling of dMRI data

3.1 Diffusion tensor model

A diffusion model for dMRI data is a model that explains the directional dependence of the data acquired for a single voxel. For an overview over many of such models see, e.g., Assemlal et al. [2011]. Such models are typically based on intra-voxel tissue properties. As a well-known example we will, in this paper, consider the diffusion tensor model [DTI; Basser et al., 1994a,b]. However, the statements in this paper can be easily transferred to other diffusion models like tensor-mixture models [Assaf and Basser, 2005, Behrens et al., 2003, Tabelow et al., 2012], higher-order tensor models [Özarslan and Mareci, 2003, Liu et al., 2004, Jensen and Helpern, 2010], or models related to the orientation-distribution function [ODF; Tuch, 2004].

The DTI model describes the directional dependence of the diffusion signal by an anisotropic Gaussian diffusion of water molecules within a voxel. For a given diffusion gradient direction g and b-value b (combining gradient strength and diffusion time etc. [Jones, 2010]) the model for a voxel i prescribes an exponential decay of the theoretical (noise-free) signal $\zeta_{b,g,i}$ in relation to a base intensity $\zeta_{0,i}$ acquired without diffusion weighting gradients:

$$\zeta_{b,g}(\theta_i) = \zeta_{0,i}\, e^{-bg^\top \mathcal{D}_i g} \tag{3.1}$$

The relation is characterized by the diffusion tensor $\mathcal{D}_i$ that belongs to the space of positive-definite symmetric 3×3 matrices $\mathcal{PD}(3)$. We denote the parameters of this model as $\theta_i = (\zeta_{0,i}, \vec{\mathcal{D}}_i)$ including the base intensity $\zeta_{0,i}$ and the vector of the six independent components of

$\mathcal{D}_i$. As we only consider modeling within a single voxel i we will henceforth drop the index i for the simplicity of notation.

Let $\lambda_1, \lambda_2, \lambda_3 \geq 0$ denote the eigenvalues of $\mathcal{D}$. Based on these, the fractional anisotropy (FA) as the most popular anisotropy measure

$$\mathsf{FA} = \sqrt{\frac{3}{2}} \sqrt{\sum_{i=1}^{3} (\lambda_i - \langle \lambda \rangle)^2 \Big/ \sum_{i=1}^{3} \lambda_i^2} \tag{3.2}$$

can be defined [Basser and Pierpaoli, 1996], where $\langle \lambda \rangle$ is the mean eigenvalue.

The expected value of the observed signal $S_{b,g}$ in the diffusion tensor model for a b-value b and a gradient direction g is given by

$$\mathbf{E}S_{b,g} = \mu(\zeta_{b,g}(\theta), \sigma_{b,g}) = \sigma_{b,g} \sqrt{\frac{\pi}{2}} \mathbf{L}_{1/2}^{(L-1)} \left(-\frac{\zeta_{b,g}^2(\theta)}{2\sigma_{b,g}^2} \right). \tag{3.3}$$

Here,

$$\mathbf{L}_{1/2}^{(L-1)}(x) = \frac{\Gamma(L + 1/2)}{\Gamma(3/2)\Gamma(L)} \mathbf{M}(-1/2, L, x)$$

denotes a generalized Laguerre polynomial that can be expressed using the confluent hypergeometric function $\mathbf{M}$. The variance of the preprocessed signal is

$$v_{bg} = C_{bg} \left[2L\sigma_{b,g}^2 + \zeta_{b,g}(\theta)^2 - \mu^2(\zeta_{b,g}(\theta), \sigma_{b,g}) \right]$$

where $C_{bg} \leq 1$ is characterizing the variance reduction due to preprocessing.

For the signal distributions emerging in dMRI their expected value (3.3) differs from the noise-free parameter ζ. Table 1 specifically illustrates that $\mu(\zeta_{b,g}(\theta), \sigma_{b,g}) > \zeta_{b,g}(\theta)$ and that the difference is decreasing with increasing ratio $\frac{\zeta_{b,g}(\theta)}{\sigma_{b,g}}$, i.e. increasing SNR.

ζ/σ	0.0	1.0	2.0	3.0	4.0	6.0	8.0
$(\mu(\zeta, \sigma) - \zeta)/\sigma$	1.25	0.55	0.27	0.17	0.13	0.084	0.063
$(\mu(\zeta, \sigma) - \zeta)/\zeta$	∞	0.55	0.14	0.058	0.032	0.014	0.008

Table 1 – *Absolute and relative discrepancy between expected value and signal depending on the ratio of signal and scale parameter for $L = 1$.*

3.2 Diffusion tensor estimation by nonlinear regression

Estimation of the true parameters θ is usually performed in the nonlinear regression model

$$S_{b,g} = \zeta_{b,g}(\theta') + \epsilon_{b,g}, \quad \mathbf{E}\,\epsilon_{b,g} = 0 \quad \mathbf{Var}\,\epsilon_{b,g} < \infty \tag{3.4}$$

solving the optimization problem

$$\hat{\theta} = (\hat{\zeta}_0, \vec{\hat{D}}) = \text{argmin}_{\theta'} \sum_{b,g} w_{b,g} \left[S_{b,g} - \zeta_{b,g}(\theta') \right]^2 \tag{3.5}$$

for some weights $w_{b,g}$. In case of small $\zeta_{b,g}(\theta)/\sigma_{b,g}$, at least for some pairs (b, g) of b-values and gradient directions with strong signal attenuation by the diffusion weighting the model (3.4) becomes inadequate, cf. Table 1. Solving (3.5) effectively means to compute an (weighted) inadequate least squares approximation (WILSA) of the expected signal $\mu(\zeta_{b,g}(\theta), \sigma_{b,g})$ within the class of functions $\mathcal{F} = \{\zeta_{b,g}(\theta'|\theta' \in \Theta)\}$ with $\Theta = \{(\zeta_0, \vec{D})|\zeta_0 \in \mathsf{R}^+, \mathcal{D} \in \mathcal{PD}(3)\}$. The properties of the weighted inadequate least squares estimate $\hat{\theta}$ are studied, e.g., in Zwanzig [1980] and Bunke and Bunke [1989]. We use the framework developed therein to investigate the effects of low SNR in dMRI for the special case of the diffusion tensor model (3.1).

Let n be the cardinality of the set of pairs (b, g) of b-values and gradient directions. Let u denote a set of positive numbers such that $0 < \kappa \le u_{b,g} \le \rho < \infty$ with $\max_{b,g} |w_{b,g} - u_{b,g}| \xrightarrow{a.s.} 0$. We use the following notation introduced in Bunke and Bunke [1989] to formulate their result in our specific situation:

$$k_\zeta(b, g) = \frac{\partial \zeta}{\partial \theta'}(b, g) \mid_{\theta' = \bar{\theta}},$$

$$^w|y - f|_n^2 = n^{-1} \sum_{b,g} w_{b,g}|y_{b,g} - f_{b,g}|^2,$$

$$^w(k, l)_n = \left(\left(n^{-1} \sum_{b,g} w_{b,g} k_i(b, g) l_j(b, g) \right)^{i=1,7}_{j=1,7} \right).$$

Under mild regularity conditions Theorem 1.1.2 in Bunke and Bunke [1989] provides the asymptotic normality of the inadequate least squares approximation (WILSA) as

$$\mathcal{L} \left\{ n^{1/2}(\hat{\theta} - \bar{\theta} - 2G(u)^{-1} {}^u(k_\zeta, \mu(\zeta(\theta), \sigma) - \zeta(\bar{\theta}))_n \right\} \to N(0, 4G(u)^{-1}C_\zeta(u)G(u)^{-1}). \tag{3.6}$$

The parameter $\bar{\theta}$ in (3.6) is the projection parameter defined as

$$\bar{\theta} = \text{argmin}_{\theta'} {}^u|\mu(\zeta(\theta), \sigma) - \zeta(\theta')|^2. \tag{3.7}$$

The asymptotic covariance matrix depends on

$$C_\zeta(u) = \lim_{n \to \infty} \sum_{b,g} v_{b,g} u_{b,g}^2 k_\zeta(b, g) k_\zeta(b, g)^T \quad \text{and}$$

$$G(u) = \left(\left(\frac{\partial^2}{\partial \theta'_i \partial \theta'_j} \lim_{n \to \infty} {}^u|\mu(\zeta_{b,g}(\theta), \sigma_{b,g}) - \zeta_{b,g}(\theta')|_n^2]|_{\theta' = \bar{\theta}} \right)^{i=1,7}_{j=1,7} \right).$$

The term $2G(u)^{-1} {}^u(k, \mu(\zeta(\theta), \sigma) - \zeta(\bar{\theta}))_n$ is needed to obtain a vanishing expectation in the limiting distribution. Bunke [1981], see also Remark 1.1.2 in Bunke and Bunke [1989], provided

a refinement of (3.6)

$$\mathcal{L}\left\{n^{1/2}(\hat{\theta} - \bar{\theta}_n)\right\} \to N(0, 4G(u)^{-1}C_\zeta(u)G(u)^{-1}). \tag{3.8}$$

using

$$\bar{\theta}_n = \operatorname{argmin}_{\theta'} {}^{w}|\mu(\zeta(\theta), \sigma) - \zeta(\theta')|^2$$

instead of $\bar{\theta}$ that avoids the correction term $2G(u)^{-1} {}^{u}(k, \mu(\zeta(\theta), \sigma) - \zeta(\bar{\theta}))_n$ in (3.6).

The difference $\bar{\theta}_n - \theta$ between the projection parameter and the true value θ in Eqn. (3.1) characterizes the non-vanishing bias due to model misspecification.

3.3 Quasi-Likelihood estimation

Unfortunately, a likelihood approach can not be used since the distribution of the preprocessed signals depends on the interpolation weights used in susceptibility correction, eddy current correction and image registration. All these interpolation steps keep the expected value of the signal in (3.3) unchanged. In this equation $2L$ are the degrees of freedom and σ the scale parameter of the distribution of the unprocessed data. The variance of the observed signal is reduced by spatial interpolation at the cost of additional spatial correlation. The model (3.3) is adequate under the assumption of a homogeneous Gaussian diffusion within the voxel. The parameter vector θ can be estimated by iteratively weighted least squares comparing the observed signal with its expectation

$$\tilde{\theta} = \operatorname{argmin}_{\theta'} \sum_{b,g} w_{b,g} \left[S_{b,g} - \mu(\zeta_{b,g}(\theta'), \sigma_{b,g})\right]^2 \tag{3.9}$$

Choosing $w_{b,g} = 1/v_{b,g}$ this corresponds to a quasi-likelihood approach that employs the variance of the unprocessed data. An alternative choice is $w_{b,g} \equiv 1$. The asymptotic distribution of the WLSE $\tilde{\theta}$ is, under mild regularity conditions, see e.g. Bunke and Schmidt [1980] or Theorem 1.1.2 in Bunke and Bunke [1989], given by

$$\mathcal{L}\left\{n^{1/2}(\tilde{\theta} - \theta)\right\} \to N(0, B(u)^{-1}C_\mu(u)B(u)^{-1}) \tag{3.10}$$

with

$$k_\mu(b, g) = \frac{\partial \mu}{\partial \theta'}(b, g) \mid_{\theta'=\theta},$$

$$B(u) = \lim_{n \to \infty} {}^{u}(k_\mu, k_\mu)_n$$

$$C_\mu(u) = \lim_{n \to \infty} \sum_{b,g} v_{b,g} u_{b,g}^2 k_\mu(b, g) k_\mu(b, g)^T.$$

The WLSE is a consistent estimate of the true parameter θ.

4 Simulations in the diffusion tensor model

In this Section we compare the estimates $\hat{\theta}$ and $\bar{\theta}$ from (3.5) and (3.9), respectively, in a controlled situation. To simulate parameter estimates that obey the assumption of a Gaussian diffusion profile (diffusion tensor model) we re-parametrized the model (3.1) using

$$\vartheta = (\zeta_0, \overrightarrow{\log \mathcal{D}}) \tag{4.1}$$

with $\log \mathcal{D} = U \operatorname{diag}(\log(\lambda)) U^T$ for an eigenvalue decomposition $\mathcal{D} = U \operatorname{diag}(\lambda) U^T$. This corresponds to using a log-Euclidean metric in the space of diffusion tensors $\mathcal{PD}(3)$, see e.g. Pennec et al. [2006], Fletcher and Joshi [2007], or Arsigny et al. [2006] and has the advantage that affine Euclidean operations on ϑ preserve the tensor properties for $\mathcal{D}$.

We considered an experiment that resembles the design used for the data in the Human Connectome project [Van Essen et al., 2013, Sotiropoulos et al., 2013a, Ugurbil et al., 2013]. The matrices $B(w), C_\mu(w), G(w)$ and $C_\zeta(w)$ were generated employing the 90 diffusion gradient direction used in the HCP on each of 3 shells, i.e., b-values of $1000\,\mathrm{s/mm}^2, 2000\,\mathrm{s/mm}^2$, and $3000\,\mathrm{s/mm}^2$ and assuming 18 non-diffusion weighted volumes corresponding to a b-value of $0\,\mathrm{s/mm}^2$.

The diffusion tensor $\mathcal{D}$ was assumed to be prolate, i.e., $\lambda_2 = \lambda_3$, with a maximal eigenvalue $\lambda_1 = 1.4 \times 10^{-3}\,\mathrm{mm}^2/\mathrm{s}$. The signal was scaled such that $\zeta_0 = 1$. We further assumed the preprocessed signal to be a weighted average of Rician distributed variables ($L_{eff} = 1$ as in the HCP) with scale parameter σ. The averages were assumed to mimic the effects of interpolation in the preprocessing steps and to lead to a variance reduction by a factor of 4. This resembles the variance reduction observed when analyzing the unprocessed and preprocessed Human Connectome data, see Section 5.

In the following simulations we sampled 100000 realizations from the asymptotic distributions (3.8) and (3.10) with covariance matrices $4G(w)^{-1}C_\zeta(w)G(w)^{-1}$ and $B(w)^{-1}C_\mu(w)B(w)^{-1}$, respectively, and projection parameter $\bar{\vartheta}$ calculated numerically under the re-parametrization (4.1).

We investigated the properties of the estimated eigenvalues and fractional anisotropy for varying (true) tensor anisotropy (FA) and SNR ($1/\sigma$). In general there are two causes of bias in the estimation of FA. The first comes from the variability of the tensor estimates and can be controlled, e.g., by increasing the number of diffusion weighted images. The second contribution is due to the use of the inadequate nonlinear regression model or a misspecification of σ. In Table 2 we report the FA values calculated from the projection parameter $\bar{\theta}$, see Eq. (3.7). The difference between the reported values and the true FA in the first row is the bias part of the FA estimate obtained from nonlinear regression that is due to model misspecification.

Figure 1 provides the boxplots of errors in estimated FA for true FA values ranging from 0.1 to 0.9 obtained from nonlinear regression (3.5) as well as from quasi-likelihood (3.9) estimates from the simulated datasets. We observed a severe negative bias in case of nonlinear regression that is, as expected, decreasing with increasing SNR ζ_0/σ. This effect is mainly due to the bias in the nonlinear regression (3.5) estimate. For small SNR and small true FA values we also observed a positive bias in the quasi-likelihood FA estimate that is caused by the variability of the tensor estimate.

σ	True FA								
	0.1	0.2	0.3	0.4	0.5	0.6	0.7	0.8	0.9
0.2	0.0446	0.0963	0.1583	0.2324	0.3215	0.4287	0.5563	0.7016	0.8534
0.1	0.0783	0.1598	0.2456	0.3378	0.4375	0.5451	0.6584	0.7740	0.8884
0.05	0.0921	0.1859	0.2815	0.3800	0.4815	0.5848	0.6890	0.7933	0.8970

Table 2 – *FA values for the projection parameter $\bar{\theta}$ in the nonlinear regression model.*
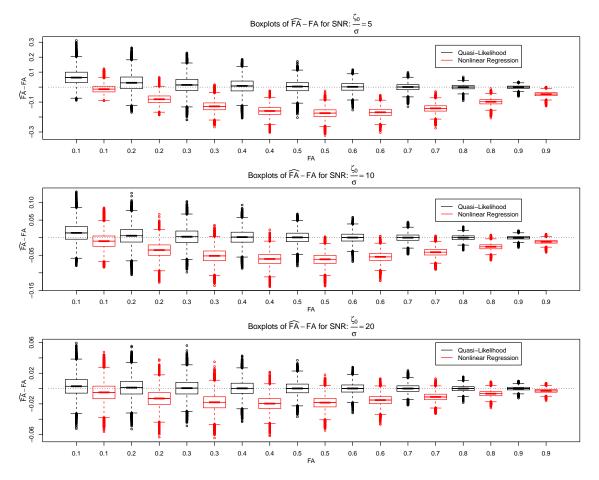

Figure 1 – *Asymptotic distribution of FA estimated by Quasi-Likelihood (black) and Nonlinear regression (red) in the diffusion tensor model with the b-value and gradient direction scheme used in the Human Connectome Project. Results are provided for FA values varying from 0.1 to 0.9 and a signal to noise in the non-diffusion weighted signal of 5, 10 and 20.*

Figure 2 provides relative errors of the estimated tensor eigenvalues for the same settings. In case of the nonlinear regression estimates we see a negative relative error in the estimated eigenvalues, with errors most severe for the largest eigenvalue and low SNR.

We also investigated the case were the data is generated by a tensor mixture model [Tabelow et al., 2012] within a voxel instead of a single diffusion tensor model (DTI). Then, both the nonlinear regression and the quasi-likelihood estimates were obtained in an inadequate model.
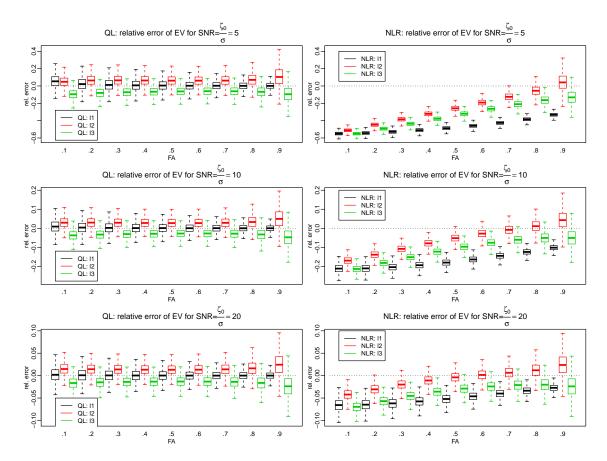
Figure 2 – *Relative errors of tensor eigenvalues estimated by Quasi-Likelihood and Nonlinear regression in the diffusion tensor model with the b-value and gradient direction scheme used in the Human Connectome Project. Results are provided for FA values varying from 0.1 to 0.9 and a signal to noise in the non-diffusion weighted signal of 5, 10 and 20.*

In all considered situations (not reported here) we saw a negative bias in estimated FA that was significantly larger in case of nonlinear regression.

5 Analysis of HCP data

To illustrate our findings with experimental MR data we used dMRI data from the Q1/Q2-release of the Human Connectome Project [Van Essen et al., 2013, Sotiropoulos et al., 2013a, Ugurbil et al., 2013].

5.1 Description of data and preprocessing

Data were generated on a customized Siemens 3T "Connectome Skyra" using a Spin-echo EPI Sequence, $TR = 5520$ ms, $TE = 89.5$ ms, flip angle $78°$, refocusing flip angle $160°$, field of view 210 mm $\times$ 180 mm (RO x PE), matrix size 168×144, slice thickness 1.25 mm, with a total of 111 slices, leading to $1.25 \times 1.25 \times 1.25$ mm^3 isotropic voxels. The acquisition

employed a multiband factor of 3, echo spacing of 0.78 ms, bandwidth 1488 Hz/Px, phase partial Fourier factor of 6/8, and b-values 1000 s/mm^2, 2000 s/mm^2, and 3000 s/mm^2. A total of 576 image volumes were obtained in six runs each utilizing three different gradient tables of 90 gradient directions plus 6 non-diffusion weighted acquisitions. Each gradient table was used once with right-to-left and left-to-right phase encoding. Image reconstruction of the raw data used SENSE1 [Sotiropoulos et al., 2013b].

Data preprocessing included intensity normalization across runs, EPI distortion (susceptibility) correction using FSL-TOPUP [Andersson et al., 2003, Smith et al., 2004], eddy-current and motion correction by FSL-EDDY, gradient nonlinearity correction, including calculation of b-value and gradient direction deviation and registration of the mean non-diffusion-weighted image to a native volume T1w image. A brain mask is available based on a freesurfer segmentation [Dale et al., 1999]. See also [Hum, 2013a,b] for more details on image acquisition and processing. We analyzed both the unprocessed as well as the preprocessed data.

5.2 Estimation of the local scale parameter for the unprocessed data

We estimated the local scale parameter σ for 192 of the 576 images (two out of the six runs) using the local adaptive noise estimation (LANE) algorithm from [Tabelow et al., 2015] as implemented in the **R** package **dti** [Tabelow and Polzehl, 2015]. LANE was applied specifying Rician noise which is appropriate for the SENSE1 reconstructed images in the considered dataset. In this method voxelwise estimates of the scale parameter σ and the intensity ζ are obtained by weighted local likelihood. To do so the procedure employs an assumption of local homogeneity for ζ and spatial smoothness of σ in an iterative multi-scale procedure, see Tabelow et al. [2015] for details. This approach is designed to recover the local homogeneity structure of ζ and describe this structure in terms of local weighting schemes that are employed in the weighted likelihood approach.

Figure 3 illustrates the results for the unprocessed data, i.e., for the data after image reconstruction before applying any artifact correction method. In the left part of the figure we provide images of estimated scale parameters for one slice of a non-diffusion weighted image and images at b-values 1000 s/mm^2, 2000 s/mm^2 and 3000 s/mm^2. The scale parameter σ is approximately constant within the brain mask and depends on the b-value. The central part of the figure provides densities of the estimated scale parameters within the brain mask for each analyzed image volume. Phase encoding direction and b-values are color-coded. The right plot in Figure 3 provides densities of the estimated SNR ζ/σ for the 192 analyzed image volumes.

We consistently observe low SNR for parts of all diffusion weighted images. The effect is most severe for high b-values leading to a high percentage of voxel with low estimated SNR, see Table 3.

5.3 Estimation of the local scale parameter for the preprocessed data

Data preprocessing, i.e., susceptibility distortion, eddy current and motion correction effectively lead to interpolation between neighboring voxel. While this does not significantly change the ex-
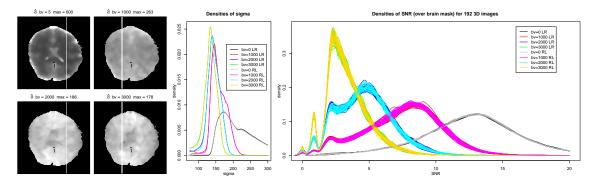
Figure 3 – *Left: Estimated local scale parameter σ in a slice of a non-diffusion weighted and three diffusion weighted images with approximate b-values 1000 s/mm^2, 2000 s/mm^2 and 3000 s/mm^2. Center: Densities of estimated σ obtained from 2 out of 6 runs (a total of 192 image volumes, 96 with right-to-left (RL) and 96 with left-to-right (LR) phase encoding directions). Right: Densities of estimated SNR ζ/σ for same volumes.*

b-value in s/mm^2	0	1000	2000	3000
run with LR phase encoding	4%	14%	38%	71%
run with RL phase encoding	3%	13%	37%	71%

Table 3 – *Percentage of voxel in brain mask with SNR less than 4.*

pected value of the local intensities it reduces, due to averaging, their variance. It also changes the signal distribution from Rician to an approximately Gaussian with expected value μ.

We estimated the local noise standard deviation and the SNR μ/σ in all 288 volumes [1] of the preprocessed data using LANE [Tabelow et al., 2015]. The results are summarized in Figure 4. Compared to the unprocessed data analyzed in the previous subsection we observed a reduction of the standard deviation by a factor of approximately 2 due to preprocessing. The SNR μ/σ is significantly increased for all b-values.

5.4 Nonlinear regression versus quasi-likelihood

We also estimated the parameters θ in the diffusion tensor model (3.1). We computed both the inadequate nonlinear regression estimate (3.5) and the quasi-likelihood estimate (3.9) from the *preprocessed* data using method `dtiTensor` from the **R**-package **dti** [Tabelow and Polzehl, 2015]. There, we used the estimated scale parameter σ determined with the *unprocessed* data, as it determines the distributional properties of the signal.

Figure 5 provides a comparison of both estimates in terms of FA differences and relative changes of the eigenvalues. We observed a significant increase in the estimated FA with the quasi-likelihood estimation in white matter together with tissue specific changes in the tensor eigenvalues. This indicates the presence of a severe bias in the nonlinear regression estimates even

---

[1] There, the RL and LR phase encoding acquisitions have been combined to a single image that is corrected for the susceptibility artifact.
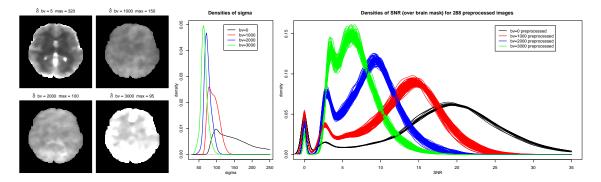
Figure 4 – *Left: Estimated local scale parameter σ in a slice of a non-diffusion weighted and three diffusion weighted images with approximate b-values 1000 s/mm^2, 2000 s/mm^2 and 3000 s/mm^2. Center: Densities of estimated σ obtained from a total of 288 preprocessed image volumes. Right: Densities of estimated SNR μ/σ for same volumes.*
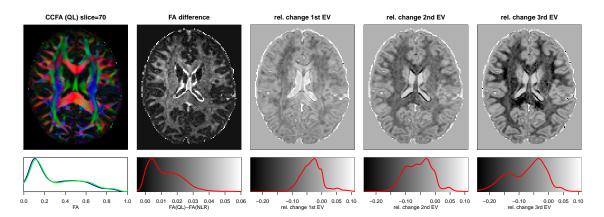

Figure 5 – *Color coded FA obtained by quasi likelihood estimation of θ, FA difference between quasi-likelihood and nonlinear regression estimates, relative changes of the three eigen-values (from left to right). The bottom row provides densities (over voxel within the brain mask) of FA (nonlinear regression estimates in blue, quasi-likelihood estimates in green), as well as the FA difference and the relative changes of the eigenvalues.*

for high quality diffusion weighted data.

6 Discussion and Conclusion

In this paper, we considered statistical problems in modeling MRI data related to low signal-to-noise ratio. Low SNR is typically observed in MR experiments with very high spatial resolution but also, e.g., in diffusion MR experiments with strong signal attenuation at high b-values. Then, the signal distribution becomes skewed with the signal expectation exceeding the nominal noiseless signal, see Table 1. Commonly applied models based on linearized (not considered here) or nonlinear regression rely on the assumption that the expected and nominal signal ζ coincide and therefore introduce a bias in the estimated model parameters.

Adequate handling of the problem requires the characterization of the distribution of signals obtained from image reconstruction by, e.g. SENSE or GRAPPA. This distribution can be usually approximated by a rescaled non-central χ-distribution, with the non-centrality parameter ζ/σ corresponding to the SNR. Preprocessing, i.e., correction for artifacts and image registration, essentially leads to a spatial signal interpolation. These are generally designed to preserve image intensity, i.e., they preserve the gap between expected and nominal signal. The resulting signal distribution depends on the interpolation weights, and is more concentrated and closer to a Gaussian distribution. An adequate model can be established matching the signal with the expected instead of the nominal signal leading to a quasi-likelihood approach. This approach relies on a reliable estimate of the scale parameter σ. The quasi-likelihood approach provides an alternative to procedures that transform the unprocessed data to achieve approximate Gaussianity as proposed in, e.g., Koay et al. [2009], Foi [2011], or Bai et al. [2015].

Using results for weighted inadequate nonlinear regression approximations from Bunke and Bunke [1989] we established an asymptotic framework to investigate both the nonlinear regression and the quasi-likelihood approach. We used the diffusion tensor model for diffusion weighted MR data to illustrate and analyze results for both approaches. Our simulations show that the bias of estimated FA and eigenvalues in the nonlinear regression approach can be severe in case of low SNR. This bias consists of two parts, a contribution from the variability of tensor estimates that could be controlled by using more diffusion weighted images and a SNR and parameter dependent bias due to model misspecification.

We then analyzed unprocessed and preprocessed data from the Human Connectome Project. We showed that the scale parameter σ can be reproducibly (over all diffusion weighted images) estimated by LANE. For the unprocessed data we observed, especially for the larger b-values, that a high percentage of voxel exhibits low SNR. The problem is hidden when analyzing the preprocessed data. We also showed that FA estimates by quasi-likelihood and nonlinear regression show substantial tissue dependent differences.

The methodology can be easily generalized to other diffusion models [Assemlal et al., 2011] or other MR acquisition protocols like MPM [Weiskopf et al., 2013].

While the bias observed in non-linear regression may be ignored in the interpretation of results for a single MR data set it severely limits interpretation in repeated time, multi-subject, and multi-side studies where scanner properties can be expected to vary.

7 Acknowledgment

References

S. Aja-Fernández and A. Tristán-Vega. Influence of noise correlation in multiple-coil statistical models with sum of squares reconstruction. *Magnetic Resonance in Medicine*, 67(2):580–585, 2012.

S. Aja-Fernández, A. Tristán-Vega, and W.S. Hoge. Statistical noise analysis in grappa using a parametrized noncentral chi approximation model. *Magnetic Resonance in Medicine*, 65(4):1195–1206, 2011.

J.L.R. Andersson, S. Skare, and J. Ashburner. How to correct susceptibility distortions in spin-echo echo-planar images: application to diffusion tensor imaging. *NeuroImage*, 20(2):870–888, 2003.

V. Arsigny, P. Fillard, X. Pennec, and N. Ayache. Log-euclidean metrics for fast and simple calculus on diffusion tensors. *Magnetic Resonance in Medicine*, 56:411–421, 2006.

Y. Assaf and P.J. Basser. Composite hindered and restricted model of diffusion (CHARMED) MR imaging of the human brain. *NeuroImage*, 27(1):48–58, 2005.

H.-E. Assemlal, D. Tschumperlé, L. Brun, and K. Siddiqi. Recent advances in diffusion MRI modeling: Angular and radial reconstruction. *Medical Image Analysis*, 15(4):369–396, 2011.

R. Bai, C.G. Koay, E. Hutchinson, and P.J. Basser. A framework for accurate determination of the T_2 distribution from multiple echo magnitude MRI images. *Journal of Magnetic Resonance*, 244:53–63, 2015.

P.J. Basser and S. Pajevic. Statistical artefacts in diffusion tensor MRI (DT-MRI) caused by background noise. *Magnetic Resonance in Medicine*, 44(1):41–50, 2000.

P.J. Basser and C. Pierpaoli. Microstructural and physiological features of tissues elucidated by quantitative-diffusion-tensor MRI. *Journal of Magnetic Resonance, Series B*, 111:209–219, 1996.

P.J. Basser, J. Mattiello, and D. Le Bihan. MR diffusion tensor spectroscopy and imaging. *Biophysical Journal*, 66:259–267, 1994a.

P.J. Basser, J. Mattiello, and D. Le Bihan. Estimation of the effective self-diffusion tensor from the NMR spin echo. *Journal of Magnetic Resonance B*, 103:247–254, 1994b.

T.E.J. Behrens, M.W. Woolrich, M. Jenkinson, H. Johansen-Berg, R.G. Nunes, S. Clare, P.M. Matthews, J.M. Brady, and S.M. Smith. Characterization and propagation of uncertainty in diffusion-weighted MR imaging. *Magnetic Resonance in Medicine*, 50:1077–1088, 2003.

I.P. Bruce and D.B. Rowe. Quantifying the statistical impact of GRAPPA in fcMRI data with a real-valued isomorphism. *IEEE Transactions on Medical Imaging*, 33(2):495–503, 2014.

I.P. Bruce, M.M. Karaman, and D.B. Rowe. A statistical examination of SENSE image reconstruction via an isomorphism representation. *Magnetic Resonance Imaging*, 29(9):1267–1287, 2011.

I.P. Bruce, M.M. Karaman, and D.B. Rowe. The SENSE-isomorphism theoretical image voxel estimation (SENSE-ITIVE) model for reconstruction and observing statistical properties of

reconstruction operators. *Magnetic Resonance Imaging*, 30(8):1143–1166, 2012.

H. Bunke. A note on parameter estimation in inadequate nonlinear regression models. *Mathematische Operationsforschung und Statistik, Series Statistics*, 12:7–11, 1981.

H. Bunke and O. Bunke, editors. *Nonlinear regression, functional relations and robust methods. Statistical methods of model building, vol. II.* Wiley, 1989.

H. Bunke and W.H. Schmidt. Asymptotic resuts on nonlinear approximation of regression functions and weighted least squares. *Mathematische Operationsforschung und Statistik, Series Statistics*, 11:3–22, 1980.

P.T. Callaghan. *Principles of Nuclear Magnetic Resonance Microscopy*. Oxford Science Publications, 1991.

A. Dale, B. Fischl, and M.I. Sereno. Cortical surface-based analysis: I. segmentation and surface reconstruction. *NeuroImage*, 9(2):179 – 194, 1999.

M. Deppe, T. Duning, S. Mohammadi, W. Schwindt, H. Kugel, S. Knecht, and E.B. Ringelstein. Diffusion-tensor imaging at 3T: detection of white matter alterations in neurological patients on the basis of normal values. *Investigative Radiology*, 42(6):338–345, Jun 2007.

M. Deppe, D. Müller, H. Kugel, T. Ruck, H. Wiendl, and S.G. Meuth. DTI detects water diffusion abnormalities in the thalamus that correlate with an extremity pain episode in a patient with multiple sclerosis. *Neuroimage Clinical*, 2:258–262, 2013.

W.A. Edelstein, G.H. Glover, C.J. Hardy, and R.W. Redington. The intrinsic signal-to-noise ratio in NMR imaging. *Magnetic Resonance in Medicine*, 3:604–618, 1986.

P.T. Fletcher and S. Joshi. Riemannian geometry for the statistical analysis of diffusion tensor data. *Signal Processing*, 87:250–262, 2007.

A. Foi. Noise estimation and removal in MR imaging: the variance-stabilization approach. In *Proc. 2011 IEEE International Symposium on Biomedical Imaging*, pages 1809–1814, 2011.

M.A. Griswold, P.M. Jakob, R.M. Heidemann, M. Nittka, V. Jellus, J. Wang, B. Kiefer, and A. Haase. Generalized autocalibrating partially parallel acquisitions (GRAPPA). *Magnetic Resonance in Medicine*, 47(6):1202–1210, 2002.

H. Gudbjartsson and S. Patz. The Rician distribution of noisy MRI data. *Magnetic Resonance in Medicine*, 34:910–914, 1995.

C.E. Hayes and P.B. Roemer. Noise correlations in data simultaneously acquired from multiple surface coil arrays. *Magnetic Resonance in Medicine*, 16(2):181–191, 1990.

R.M. Henkelman. Measurement of signal intensities in the presence of noise in MR images. *Medical Physics*, 12(2):232–233, 1985.

WU-Minn HCP Quarter 1 (Q1) Release: Reference Manual. Human Connectome Project, 5 March 2013a.

WU-Minn HCP Quarter 1 (Q2) Data Release: Reference Manual. Human Connectome Project, 5 March 2013b.

J.H. Jensen and J.A. Helpern. MRI quantification of non-Gaussian water diffusion by kurtosis

analysis. *NMR in Biomedicine*, 23(7):698–710, 2010.

H. Johansen-Berg and T.E.J. Behrens, editors. *Diffusion MRI: From Quantitative Measurement to In-Vivo Neuroanatomy*. Academic Press, 2009.

D.K. Jones, editor. *Diffusion MRI: Theory, Methods, and Applications*. Oxford University Press, 2010.

D.K. Jones and P.J. Basser. "Squashing peanuts and smashing pumpkins": How noise distorts diffusion-weighted MR data. *Magnetic Resonance in Medicine*, 52:979–993, 2004.

I. Kleffner, M. Deppe, S. Mohammadi, H. Schiffbauer, N. Stupp, H. Lohmann, P. Young, and E.B. Ringelstein. Diffusion tensor imaging demonstrates fiber impairment in Susac syndrome. *Neurology*, 70:1867–1869, 2008.

C.G. Koay, E. Ozarslan, and P.J. Basser. A signal transformational framework for breaking the noise floor and its applications in MRI. *Journal of Magnetic Resonance*, 197(2):108–119, 2009.

Ch. Liu, R. Bammer, B. Acar, and M.E. Moseley. Characterizing non-Gaussian diffusion by using generalized diffusion tensors. *Magnetic Resonance in Medicine*, 51(5):924–937, 2004.

S. Mohammadi, H.E. Möller, H. Kugel, D.K. Müller, and M. Deppe. Correcting eddy current and motion effects by affine whole-brain registrations: evaluation of three-dimensional distortions and comparison with slicewise correction. *Magnetic Resonance in Medicine*, 64(4):1047–1056, 2010.

E. Özarslan and T.H. Mareci. Generalized diffusion tensor imaging and analytical relationships between diffusion tensor imaging and high angular resolution diffusion imaging. *Magnetic Resonance in Medicine*, 50:955–965, 2003.

X. Pennec, P. Fillard, and N. Ayache. A Riemannian framework for tensor computing. *International Journal of Computer Vision*, 66:41–66, 2006.

C. Pierpaoli and P.J. Basser. Toward a quantitative assessment of diffusion anisotropy. *Magnetic Resonance in Medicine*, 36(6):893–906, 1996.

K.P. Pruessmann, M. Weiger, M.B. Scheidegger, and P. Boesiger. SENSE: sensitivity encoding for fast MRI. *Magnetic Resonance in Medicine*, 42(5):952–962, 1999.

S.O. Rice. *Mathematical Analysis of Random Noise*. Number Monograph B-1589. Bell Telephone Labs., Inc., New York, N.Y., 1944.

P.B. Roemer, W.A. Edelstein, C.E. Hayes, S.P. Souza, and O.M. Mueller. The NMR phased array. *Magnetic Resonance in Medicine*, 16(2):192–225, 1990.

L. Ruthotto, H. Kugel, J. Olesch, B. Fischer, J. Modersitzki, M. Burger, and C.H. Wolters. Diffeomorphic susceptibility artifact correction of diffusion-weighted magnetic resonance images. *Physics in Medicine and Biology*, 57(18):5715–5731, 2012.

S.M. Smith, M. Jenkinson, M.W. Woolrich, C.F. Beckmann, T.E.J. Behrens, H. Johansen-Berg, P.R. Bannister, M. De Luca, I. Drobnjak, D.E. Flitney, R. Niazy, J. Saunders, J. Vickers, Y. Zhang, N. De Stefano, J.M. Brady, and P.M. Matthews. Advances in functional and structural MR image analysis and implementation as FSL. *NeuroImage*, 23(S1):208–219, 2004.

S.N. Sotiropoulos, S. Jbabdi, J. Xu, J.L. Andersson, S. Moeller, E.J. Auerbach, M.F. Glasser, M. Hernandez, G. Sapiro, M. Jenkinson, D.A. Feinberg, E. Yacoub, C. Lenglet, D.C. Van Essen, K. Ugurbil, and T.E.J. Behrens. Advances in diffusion MRI acquisition and processing in the Human Connectome Project. *NeuroImage*, 80:125–143, 2013a.

S.N. Sotiropoulos, S. Moeller, S. Jbabdi, J. Xu, J.L. Andersson, E.J. Auerbach, E. Yacoub, D. Feinberg, K. Setsompop, L.L. Wald, T.E.J. Behrens, K. Ugurbil, and C. Lenglet. Effects of image reconstruction on fibre orientation mapping from multichannel diffusion MRI: Reducing the noise floor using SENSE. *Magnetic Resonance in Medicine*, 70(6):1682–1689, 2013b.

K. Tabelow and J. Polzehl. *dti: Analysis of diffusion weighted imaging (DWI) data*, 2015. URL `http://CRAN.R-project.org/package=dti`. R package version 1.2-3.

K. Tabelow, H.U. Voss, and J. Polzehl. Modeling the orientation distribution function by mixtures of angular central Gaussian distributions. *Journal of Neuroscience Methods*, 203(1):200–211, 2012.

K. Tabelow, H.U. Voss, and J. Polzehl. Local estimation of the noise level in MRI using structural adaptation. *Medical Image Analysis*, 20(1):76–86, 2015.

D.S. Tuch. Q-ball imaging. *Magnetic Resonance in Medicine*, 52:1358–1372, 2004.

K. Ugurbil, J. Xu, E.J. Auerbach, S. Moeller, A.T. Vu, J.M. Duarte-Carvajalino, C. Lenglet, X. Wu, S. Schmitter, P.F. Van de Moortele, J. Strupp, G. Sapiro, F. De Martino, D. Wang, N. Harel, M. Garwood, L. Chen, D. A. Feinberg, S.M. Smith, K.L. Miller, S.N. Sotiropoulos, S. Jbabdi, J.L.R. Andersson, T.E.J. Behrens, M.F. Glasser, D.C. Van Essen, and E. Yacoub. Pushing spatial and temporal resolution for functional and diffusion MRI in the Human Connectome Project. *NeuroImage*, 80:80 – 104, 2013.

D.C. Van Essen, S.M. Smith, D.M. Barch, T.E.J. Behrens, E.Yacoub, and K. Ugurbil. The WU-Minn Human Connectome Project: An overview. *NeuroImage*, 80:62 – 79, 2013.

N. Weiskopf, J. Suckling, G. Williams, M. M. Correia, B. Inkster, R. Tait, C. Ooi, E. T. Bullmore, and A. Lutti. Quantitative multi-parameter mapping of R1, PD(*), MT, and R2(*) at 3T: a multi-center validation. *Frontiers in Neuroscience*, 7(95), 2013.

N. Weiskopf, M. F. Callaghan, O. Josephs, A. Lutti, and S. Mohammadi. Estimating the apparent transverse relaxation time (R2*) from images with different contrasts (ESTATICS) reduces motion artifacts. *Frontiers in Neuroscience*, 8(278), 2014.

S. Zwanzig. Inadequate least squares. *Mathematische Operationsforschung und Statistik, Series Statistics*, 11:23–48, 1980.